



ELSEVIER

journal homepage: [www.elsevier.com/locate/jmatprotec](http://www.elsevier.com/locate/jmatprotec)

# Computational analysis of injection-molding residual-stress development in direct-adhesion polymer-to-metal hybrid body-in-white components

M. Grujicic<sup>a,\*</sup>, V. Sellappan<sup>a</sup>, B. Pandurangan<sup>a</sup>, G. Li<sup>a</sup>, A. Vahidi<sup>a</sup>, Norbert Seyr<sup>b</sup>, Marc Erdmann<sup>c</sup>, Jochen Holzleitner<sup>c</sup>

<sup>a</sup> International Center for Automotive Research CU-ICAR, Department of Mechanical Engineering, Clemson University, Clemson, SC 29634, United States

<sup>b</sup> BMW Group Forschung und Technik, Hanauer Straße 467, 80788 München, Germany

<sup>c</sup> BMW AG, Forschungs- und Innovationszentrum, Knorrstraße 147, 80788 München, Germany

## ARTICLE INFO

### Article history:

Received 28 July 2007

Received in revised form

13 September 2007

Accepted 16 September 2007

### Keywords:

Polymer metal hybrids

Residual stresses

Warping

Automotive structural components

## ABSTRACT

To overcome some of the main limitations of the current polymer metal hybrid (PMH) technologies, a new approach, the so-called “direct-adhesion” PMH process, has been recently proposed [Grujicic, M., Sellappan, V., Arakere, G., Seyr, N., Erdmann, M., in press. Computational feasibility analysis of direct-adhesion polymer-to-metal hybrid technology for load-bearing body-in-white structural components, *J. Mater. Process. Technol.*]. Within this approach, the necessary level of polymer-to-metal mechanical interconnectivity is attained through the use of polymer-to-metal adhesion promoters. Such promoters are applied to the metal stamping prior to their placement into the injection mold for plastic-subcomponent injection molding. The resulting enhanced polymer-to-metal adhesion affects the way injected plastic develops residual stresses while it is cooled from the plastic-melt temperature down to room temperature. In the present work, injection-molding mold-filling and material-packing analyses are combined with a structural analysis involving polymer/metal adhesion analysis to assess the extent of residual stresses and warping in a prototypical direct-adhesion PMH component. The magnitude and the distribution of such stresses and distortions are critical for the component assembly, performance and durability. The results obtained show that adhesion at the metal-stamping/plastics-subcomponent interfaces, whose presence is the bases for the direct-adhesion PMH technology, has a profound effect on the distribution and magnitude of residual stresses/distortions in the PMH component and that it must be taken into account when the component and its manufacturing processes are being designed.

© 2007 Elsevier B.V. All rights reserved.

## 1. Introduction

While metals and plastics are typically fierce competitors in automotive manufacturing, the polymer-metal-hybrid

(PMH) design technologies try to take full advantage of the two classes of materials by combining them in a singular component/sub-assembly. Several patented PMH design/manufacturing technologies have already proven their abil-

\* Corresponding author at: 241 Engineering Innovation Building, Clemson University, Clemson, SC 29634-0921, United States. Tel.: +1 864 656 5639; fax: +1 864 656 4435.

E-mail address: [mica.grujicic@ces.clemson.edu](mailto:mica.grujicic@ces.clemson.edu) (M. Grujicic).  
0924-0136/\$ – see front matter © 2007 Elsevier B.V. All rights reserved.  
doi:10.1016/j.jmatprotec.2007.09.059

ity to allow the automotive original equipment manufacturers (OEMs) to engage flexible assembly strategies, decrease capital expenditures and reduce labor required to manufacture a vehicle. The key feature of PMH structures is that the materials employed complement each other so that the resulting hybrid material can offer structural performance which is not present in either of the two constituent materials independently. Among many technical and economic benefits associated with the use of the PMH technologies, the following appear to be the most important: (a) reduction of the number of components; (b) production of the integrated components ready to assemble; (c) weight reduction compared to the traditional all-metal solutions; (d) additional design and styling freedom; (e) production of in-mold features like brackets, bosses and attachment points; (f) safety improvement due to lowered center of gravity of the vehicle; (g) a major (several fold) increase in the bending strength of stamped metal sections. This effect is well understood and is attributed to the plastic subcomponent which forces the metal to maintain its cross-section properties throughout the loading cycle and delays the onset of failure due to localized buckling; and (h) improved damping in the acoustic range (relative to their all-steel counterparts, often as high as four times lower initial decibel reading measured in a simple hammer-strike test).

The main PMH technologies currently being employed by the automotive OEMs and suppliers can be grouped into three major categories: (a) injection over-molding technologies; (b) metal over-molding technologies combined with secondary joining operations; and (c) adhesively bonded PMH structures. Since these were reviewed in great detail in our recent work (Grujicic et al., *in press*), they will be only briefly described in this section.

In the injection over-molding process (originally developed and patented by Bayer (Zoellner and Evans, 2002)), a metal-stamping profile is placed in an injection mold and polymer (typically glass fiber reinforced nylon) is injected around the profile. The plastic wraps around the edges of the sheet metal and/or through carefully designed extruded holes or buttons. There are no secondary operations required and the drawing oils/greases do not need to be removed from the metal stamping.

In the metal over-molding PMH technology (developed and patented by Rhodia (Plastic-Metal Hybrid Material, 2007)), a steel stamping is placed in an injection mold in order to coat its underside with a thin layer of reinforced nylon. In a secondary operation, the polymer-coated surface of the metal insert is ultrasonically welded to an injection molded nylon subcomponent. In this process, a closed-section structure with continuous bond lines is produced which offers a high load-bearing capability. The hollow core of the part permits functional integration-like cable housings and air or water channels.

In the adhesively bonded PMHs (developed and patented by Dow Automotive (Recktenwald, 2005)), glass-fiber reinforced poly-propylene is typically joined to a metal stamping using Dow's proprietary low-energy surface adhesive (LESA). The acrylic-epoxy adhesive does not require pre-treating of the low surface-energy poly-propylene and is applied by high-speed robots. Adhesive bonding creates continuous bond lines, minimizes stress concentrations and acts as a buffer which absorbs

contact stresses between the metal and polymer subcomponents. Adhesively bonded PMHs also enable the creation of closed-section structures which offer high load-bearing capabilities and the possibility for enhanced functionality of hybrid parts (e.g. direct mounting of air bags in instrument-panel beams or incorporation of air or water circulation inside door modules).

While the aforementioned PMH technologies have been widely used in various non-structural and load-bearing automotive components, it is well established that they, nevertheless, display some serious shortcomings. For example, to maintain the structural integrity of the part, the holes needed for polymer-to-metal interlocking in the injection over-molding process are not allowed. Similarly, edge over-molding of the stamping may be restricted. In the case of adhesively bonded PMHs, the adhesive cost, long curing time and limited ability of the adhesive to withstand aggressive chemical and thermal environments encountered in the paint-shop during body-in-white (BIW) pretreatment and E-coat curing may create defective PMH components. Consequently, alternative lower-cost PMH technologies for structural load-bearing BIW components which are compatible with the BIW manufacturing process chain are being sought.

One of such technologies, which is the subject of the present work, is the so-called direct-adhesion PMH (DA-PMH) technology in which the joining between the metal and thermo-polymer subcomponents is attained through direct adhesion of injection-molded thermoplastics to the metal without the use of interlocking rivets/over-molded edges or structural adhesives (Grujicic et al., *in press, submitted for publication-a*). There are several potential advantages offered by this technology over the ones discussed above: (a) polymer-to-metal adhesion strengths (20–30 MPa) comparable with those obtained in the case of thermo-setting adhesives are feasible but only at a small fraction of the manufacturing cycle time; (b) the shorter cycle time and the lack of use of an adhesive allow for more economical PMH-component production; (c) unlike the adhesive-bonding technology, joining is not limited to simple and non-interfering contact surfaces; (d) reduced possibility for entrapping air in undercuts of a complex surface; (e) no holes for the formation of interlocking rivets are required and, hence, structural integrity of the part is not compromised; and (f) overall reduction in the constraints placed upon the design complexity of the PMH component.

In a typical DA-PMH process, selective portions of the metal stamping are degreased and coated with an adhesion promoter before the stamping is placed into the injection mold. Upon the injection of the molten plastics into the mold cavity and following a brief material packing stage, the plastics begin to contract (due to cooling). In a conventional injection over-molding process, no significant adhesion exists between the metal stamping and the plastic injection molded subcomponent. Consequently, the in-mold residual stresses tend to develop mainly as a result of non-uniform cooling, large differences in the polymer-subcomponent wall thickness and the level of material packing, as well as due to the restrictions imposed to the polymer subcomponent by the mold during shrinkage. In the case of a DA-PMH process, on the other hand, injected polymer adheres to the metal stamping and it is not

free to detach itself from the stamping wall as the polymer cools and shrinks. This phenomena represents yet another source for in-mold (and post-ejection) residual stresses and needs to be addressed since the presence of residual stresses and the associated part warping may seriously compromise both the assembly process and the component performance and durability.

In the present work, a procedure is developed for determination of the residual stresses and warping/shrinkage within a prototypical load-bearing automotive BIW DA-PMH component. The procedure combines a set of mold-filling, material-packing and part-cooling analyses (associated with the DA-PMH fabrication process) with a part post-ejection thermo-mechanical structural analysis which accounts for the presence of adhesion at the polymer/metal contact surfaces.

The organization of the paper is as follows: an overview of the geometrical, material and structural models and the computational procedures is presented in Section 2. The results obtained in the present work are presented and discussed in Section 3. The main conclusions resulting from the present work are summarized in Section 4. A brief discussion of the “process-zone” model used to represent adhesion at the metal-stamping/polymer-subcomponent interfaces is presented in Appendix A.

## 2. Problem formulation and computational analysis

### 2.1. Definition and geometrical modeling of a prototypical automotive BIW

#### 2.1.1. Load-bearing structural PMH component

A typical load-bearing injection-over-molded PMH component is shown in Fig. 1. It consists of a flanged U-shape stamping with a number of holes and an injection molded plastic subcomponent. The plastic subcomponent consists of a number of ribs, and is attached to the metallic stamping via the injection-molded plastic rivets and over-molded stamping-flange edges. As mentioned earlier, the introduction of holes in the stamping (in order to enable the formation of interlocking rivets via injection molding) may, in general compromise the structural integrity of the component and is, hence, generally undesirable. Furthermore, since stamping flanges are often needed for joining the component to its neighbors, they may not be accessible to the plastics to form over-molded edges. Under such condition the use of polymer-to-metal DA-PMH approach is preferred. A typical load-bearing BIW DA-PMH component is displayed in Fig. 2. There are no holes in the metallic stamping and the stamping edges are not over-molded. Instead, the metallic stamping contains a series of grooves (produced by a separate stamping process). These grooves are introduced to help polymer-to-metal interlocking and to provide a larger contact surface area for polymer-to-metal adhesion. As mentioned earlier, to facilitate polymer-to-metal adhesion, an adhesion promoter is often sprayed into the grooves prior to placing the metal stamping into injection mold.

The polymer-to-metal DA-PMH component depicted in Fig. 2 will be considered as a prototypical component fab-

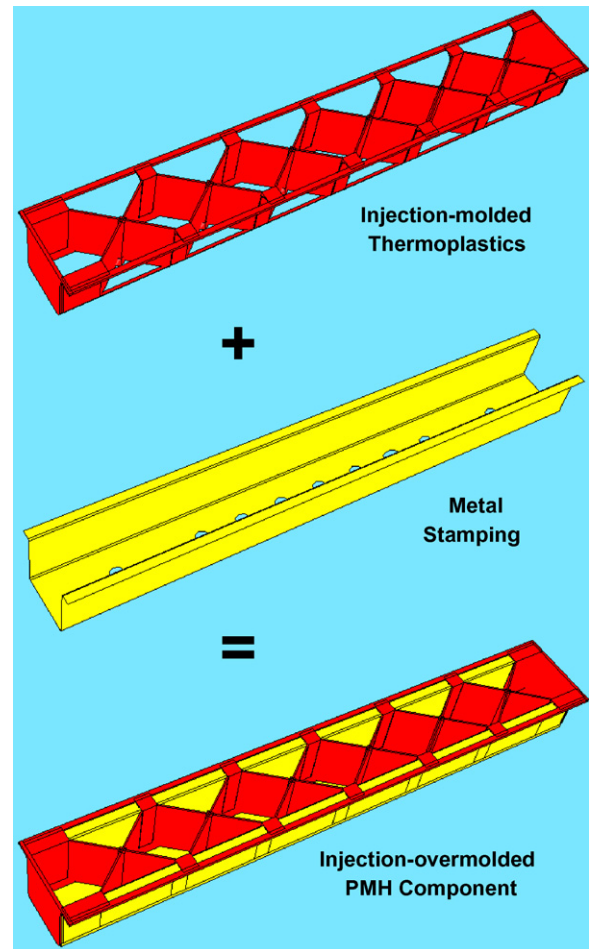


**Fig. 1 – Exploded and integrated views of a prototypical injection-over-molded polymer metal hybrid (PMH) load-bearing automotive component.**

ricated using this PMH technology and will be analyzed in the remainder of the paper. The important dimensions of the prototypical PMH component are indicated in Fig. 2. The metal stamping is set to have a uniform thickness of 1mm and to be made of a dual-phase steel with the following thermo-mechanical properties: Young's modulus,  $E = 210$  GPa, Poisson's ratio,  $\nu = 0.3$ , yield strength,  $\sigma_y = 350$  MPa, linear strain-hardening tangent modulus,  $h = 600$  MPa, linear thermal expansion coefficient,  $\alpha = 12.4 \times 10^{-6}$ . The plastic subcomponent is made of widely used Durethan BKV 130 H2.0 (a 30 wt.% glass-fiber filled Nylon 6, elastomer-modified and heat-age resistance enhanced). An average plastics subcomponent wall thickness of 1.5mm was selected to ensure complete mold filling under the standard process setting of the injection-molding machine used. In addition, to reduce the possibility for part-sticking to the mold and facilitate part ejection, a three draft angle in the direction of mold travel was applied to each face of the plastics.

The following rheological and thermal properties of Durethan BKV 130 H2.0 were used in the injection-molding mold-filling, material-packing and part cooling analysis: the viscosity is shear-rate and temperature dependent and was defined using the cross-WLF model as presented in

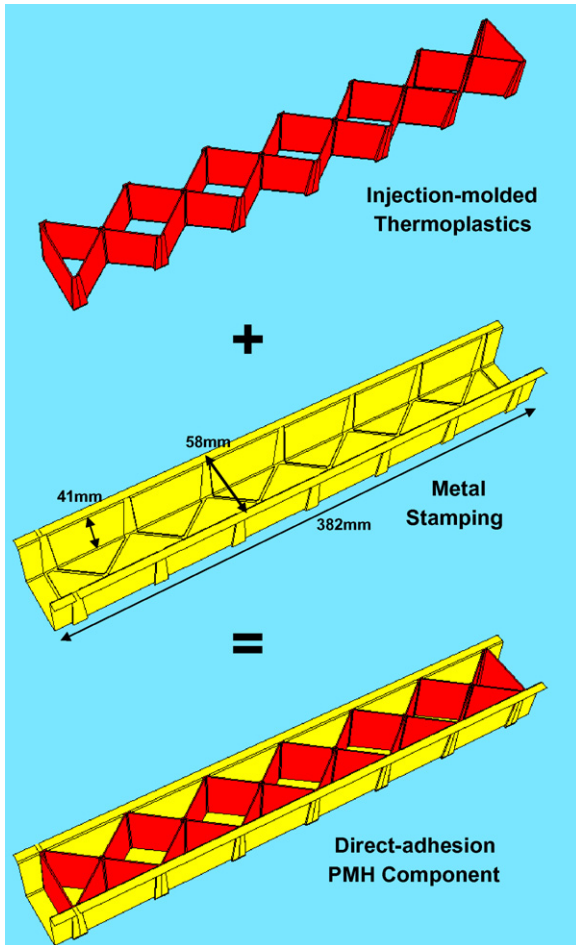


**Fig. 2 – Exploded and integrated views of a prototypical polymer-to-metal direct-adhesion polymer metal hybrid (PMH) load-bearing automotive component.**

our previous work (Grujicic et al., in press), specific heat,  $C_p = 1909 \text{ J/kgK}$ , thermal conductivity,  $k = 0.14 \text{ W/mK}$ , glass transition temperature,  $T_{\text{trans}} = 479.0 \text{ K}$ . Likewise, the following thermo-mechanical properties were used in the structural mechanics analysis of the PMH part warping/shrinking and residuals-stress development within the part: Young's modulus,  $E = 7 \text{ GPa}$ , Poisson's ratio,  $\nu = 0.4$ , yield strength,  $\sigma_y = 150 \text{ MPa}$ , linear strain-hardening tangent modulus,  $h = 100 \text{ MPa}$ , linear thermal expansion coefficient,  $\alpha = 4 \times 10^{-5}$ . It should be noted, however, that the thermo-mechanical properties for Durethan BKV 130 H2.0 given above pertain to the properties of this material in its as-received (isotropic) condition. The actual properties used in the thermo-mechanical analyses were both anisotropic and non-uniform throughout the part and were obtained by combining the mold-filling results pertaining to the local orientation of the glass-fibers with a rule-of-mixture computational scheme for determination of the effective (two-phase) material properties. A more detailed account of this procedure is given in next section.

As mentioned earlier, to enhance polymer-to-metal adhesion, an adhesion promoter is often used in the polymer-to-metal DA-PMH technologies. In the present work, it is

assumed that an adhesion promoter is used; however, its use is included only implicitly into the thermo-mechanical analysis in the present work. In other words, no separate “geometrical part” was created to represent the adhesion-promoter layer. Instead, its effect on enhancing polymer-to-metal adhesion is included by creating an adhesion interface between the polymer and metal. This adhesion interface is characterized by a traction-separation law whose main parameters are the adhesion strengths (i.e. a normal and two shear interfacial stresses at which polymer/metal decohesion/de-bonding begins to take place; the corresponding normal separation and shear displacements and the resulting normal and shear works of decohesion). Since both normal and shear decohesion modes are generally represented using a “universal” traction-separation law (Grujicic et al., submitted for publication-b), only two sets of parameters mentioned above are independent (e.g. for the normal separation mode, the work of normal decohesion is functionally related to the normal adhesion strength and to the critical (normal) polymer/metal interfacial separation). Following our previous work (Grujicic et al., submitted for publication-b), typical values are used for the normal adhesion strength,  $\sigma_n = 10 \text{ MPa}$ , shear adhesion strength,  $\sigma_{\text{sh}} = 10 \text{ MPa}$ , critical normal separation,  $d_n = 5 \text{ nm}$ , and critical shear displacement,  $d_{\text{sh}} = 25 \text{ nm}$ . A more detail description of the interfacial separation (i.e. decohesion) law used in the present work and the finite elements used to represent this law in the thermo-mechanical analysis is presented in Appendix A.

## 2.2. Pre-processing of PMH component model for mold-filling and thermo-mechanical analyses

Before computational analyses of the mold-filling and material packing stages of the prototypical PMH component fabrication process by injection over-molding can be carried out, geometrical models for the metal stamping and plastics subcomponent had to be constructed. This was done using CATIA, a computer-aided design (CAD) package from Dassault Systems (CATIA, 2007). Next, the geometrical models had to be properly meshed and pre-processed (i.e. locations of the injection gates had to be specified, the thermal conditions at the metal-stamping/plastic-subcomponent interface and metal stamping/mold interface had to be defined, etc.). Some of the main aspects of the pre-processing procedure are discussed in the remainder of this section.

After a CAD model of the metal stamping is generated, it is meshed. To meet the requirements of the mold-filling/packing computer program, Moldflow Plastics Insight 6.1 (Moldflow, for short) from Moldflow Corporation (Moldflow Plastics Insight, 2006) used in the present work, the metal stamping is discretized using ca. 120,000 triangular three-node first-order single-layer (shell) elements with an average edge length of ca. 1.0 mm.

In order to properly model the development of residual stresses within the PMH part and, specifically, in order to model the metal-stamping grooves, the polymer subcomponent is modeled as a solid part and discretized using tetrahedron four-node first-order (continuum) elements. To ensure a perfect mesh matching at the metal/polymer interfaces, the tetrahedron edge length was also kept around 1.0 mm.

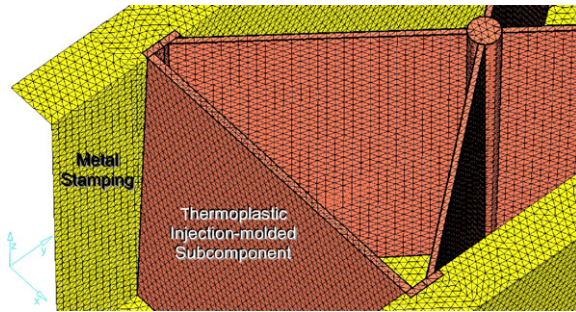


**Fig. 3 – Triangular mesh used for discretization of the metal stamping and tetrahedron mesh used for discretization of the injection-molded thermoplastic subcomponent.**

The triangular mesh used to discretize the metal stamping and the tetrahedron mesh used to discretize the thermoplastic subcomponent for a portion of the PMH component are depicted in Fig. 3. As mentioned earlier, the two meshes match perfectly across the metal-stamping/polymer-subcomponent contact interfaces.

The presence of mesh matching at the metal/plastic interfaces is highly critical since the coincident metal- and plastic-part nodes are used to construct a set of interfacial cohesion elements. There were XXX such elements in the model and they were all triangular-prism six-node traction-separation interfacial elements, Appendix A.

All the aspects of pre-processing described above and the ones presented in the remainder of this section were carried out using Hypermesh program from Altair engineering Inc. (Hypermesh, 2007). For the injection-mold filling/packing simulations, the remainder of the pre-processing included: placement of the injection points, definition of thermal boundary conditions at the metal-stamping/plastic-subcomponent and metal-stamping/tool interfaces, definition and application of the rheological and thermal properties of the participating materials, and specification of the injection-molding process parameters (e.g. plastic-melt temperature, injection flow rate, velocity/pressure switchover, packing-stage duration, part-ejection condition, etc.). Once the pre-processing procedure is completed within Hypermesh, a Moldflow input file (in the .udm format) is created and imported in the Moldflow.

As far as the pre-processing procedure for the thermo-mechanical analysis is concerned, it included the construction of the interfacial cohesion zone, thermo-mechanical material property specification, definition of the initial and boundary conditions, and loading. As mentioned earlier, the interaction between melt flow and glass-fiber reinforcements lead to the alignment of the fibers with the local flow direction, and, in turn, to the anisotropy in plastic-material thermo-mechanical properties. The information regarding the spatial distribution of the (anisotropic) material properties resulting from the Moldflow mold-filling /packing calculations (stored in a .xml type file) is converted using a general mathematical package Matlab (MATLAB, 2006) into a material-data file. The syntax of the material file was made consistent with the requirements of Abaqus/Standard (ABAQUS, 2006), the finite element program used in the present thermo-mechanical analysis of

residual-stress development. Following the same procedure, the spatial distribution of temperature within the plastics subcomponent and metal stamping attained using the Moldflow set of analyses at the end of the packing stage are exported as a temperature initial-condition file consistent with the Abaqus initial-condition data file format. As far as the boundary conditions are concerned, six degrees of freedom for one of the metal-stamping nodes are constrained to prevent the translation and rotation of the PMH part.

Upon the completion of the pre-processing procedures, for each case, a mold-filling/material-packing analysis is carried out to determine the spatial distributions of the (anisotropic) thermo-mechanical material properties and of the temperature. These results are then imported into Abaqus and a static thermo-mechanical analysis is carried out in order to: (a) determine the spatial distribution of residual stresses during the part cool-down to room temperature and (b) establish if decohesion/de-bonding has taken place at the plastic/metal interfaces and to what extent. It should be noted that, in the procedure described above, it is assumed that, due to the presence of high packing pressures, shrinkage of the plastic does not take place during the filling and packing stages of the injection-molding process.

### 2.3. Modeling of injection-molding fabrication of BIW polymer metal hybrid

#### 2.3.1. Structural component

Fabrication of the PMH structural components by thermo-plastics injection molding is a widely used in the automotive industry. A typical PMH injection-molding process involves the following distinct stages: (a) *metal stamping(s) placement* into the mold; (b) *filling* of the mold with molten thermoplastics; (c) *packing*—the injection of additional plastic material into the mold under high pressure to compensate for the cooling-induced volumetric shrinkage of the plastics; (d) *cooling* which gives rise to the solidification of the plastic material residing in the mold; (e) *ejection* of the PMH part/component from the mold after the plastics has solidified. During the filling, packing and cooling stages of the PMH injection-molding process, the material(s) (in particular the plastics) is subjected to complex thermo-mechanical loading which gives rise to the changes in local specific volume (density) and part shape, as well as to the development of the *in-mold* residual stresses in the part. In other words, while the PMH part resides in the mold, its (thin-wall) plastic subcomponent is constrained within the mid-plane causing the (residual, built-in) stresses to develop in the part during solidification of the plastics. Upon ejection, these stresses tend to relax (at least partially) causing distortion/warping and further shrinkage of molded part. Additional warping and shrinking of the part occurs during cooling of the ejected molded part from the ejection temperature down to the room temperature.

To take into account the fact that the PMH injection molded plastic subcomponent, analyzed in the present work, was made of glass-fiber filled thermo-plastics, and hence, may present some challenges during mold filling, possess residual stresses at the moment of component ejection from the mold and contain a heterogeneous, anisotropic material and a non-

uniform spatial distribution of the temperature, the following analyses were conducted: (a) determination of the optimal placement and the optimal number of plastics-injection points; (b) mold-filling analysis to obtain the filling time and spatial distribution of the glass-fiber orientation throughout the plastics subcomponent; and (c) plastic-material packing and cooling analyses to ensure that the mold-cavity is completely filled with the plastics at the instant of PMH part ejection from the mold. As mentioned earlier, all of these analyses were carried out using Moldflow Plastics Insight 6.1 (Moldflow Plastics Insight, 2006). To conduct the subsequent thermo-mechanical analysis of the residual-stress development and part shrinkage/warping, the following results obtained using Moldflow were passed to Abaqus/Standard (ABAQUS, 2006): (a) spatial distribution of the plastic-material orthotropic mechanical properties (Young's moduli:  $E_{11}$ ,  $E_{22}$ , and  $E_{33}$ ; Shear moduli:  $G_{12}$ ,  $G_{13}$ , and  $G_{23}$ ; and Poisson's ratio:  $\nu_{12}$ ,  $\nu_{13}$ , and  $\nu_{23}$ , where direction 1 coincides with the local glass-fiber directions), (b) spatial distribution of the plastic material orthotropic thermo-mechanical properties (thermal expansion coefficient,  $\alpha_1$ ,  $\alpha_2$ , and  $\alpha_3$ ), (c) spatial distribution of the local-to-global rotation matrices, and (d) spatial distribution of the temperature through the entire PMH part.

Since the detail for all the Moldflow-based analyses listed above were overviewed in great details in our recent work (Grujicic et al., in press), only a brief discussion of each will be given in the remainder of this section.

### 2.3.2. Injection-molding process parameters and settings

In the injection-molding analysis carried out in the present work, it was assumed that a Netstal commercial injection-molding machine Model 4200H-2150 is used with the following specifications: (a) the injection unit—maximum machine injection stroke = 248 mm, maximum machine injection rate = 5024 cm<sup>3</sup>/s, machine screw diameter = 80 mm; (b) the hydraulic unit—maximum machine hydraulic pressure = 17.5 MPa, intensification ratio = 10.0, machine hydraulic response time = 0.2 s; and (c) the clamping unit—maximum machine clamp force = 3800 t. Also the injection molding is assumed to be done under the following process parameters: *filling stage*—melt temperature = 563 K, injection rate = 400 cm<sup>3</sup>/s, velocity/pressure switchover at 99% volume filled; *packing stage*—time = 10 s, pressure = 80 MPa; *cooling stage*—mold surface temperature = 363 K, ejection temperature = 458 K, fraction of solid phase at ejection = 1.0; *mold material*—tool steel P20; *thermoplastics material*—Durethan BKV 130 H2.0 (an elastomer-modified Nylon 6 filled with 30 wt.% of glass-fibers and heat-age stabilized).

## 2.4. Optimal placement and number of injection points

Before simulations of the injection-molding process can be carried out, the optimal placement and the number of injection points has to be determined. The gate location analysis employed in the present work uses the part geometry, the selected material and the specified process settings and relies on the following criteria: molding feasibility and the achievement of balanced flow, so that areas furthest away from the gate(s) (i.e. injection point(s)) are filled at approximately

the same time (Moldflow Plastics Insight, 2006). To ensure that small enough plastics-wall-thicknesses can be injection molded, two gates (one attached to the second and the other to the fifth rib x-shaped intersection) were utilized in the present work, Fig. 2.

### 2.4.1. Mold filling analysis

The mold filling process is governed by the mass, momentum and energy conservation equations, which were reviewed in our recent work (Grujicic et al., in press). When injection molding of thermo-plastics filled with fibers is considered, as is the present case, the flow field is generally assumed to be independent of the orientation distribution of the fibers. In other words, the mold-filling and packing analyses are decoupled from the fiber orientation analysis. This assumption is strictly justified only in the case of injection molding of the thin-walled parts, as is the present case, in which the fibers are oriented nearly parallel to the mid-plane and, hence, their interaction with the melt flow is limited (Grujicic et al., in press; Lipscomb et al., 1988; Rosenberg et al., 1990; Zheng, 1991; Phan-Thien et al., 1991; Phan-Thien and Graham, 1991; Altan et al., 1992). The conditions which have to be satisfied in order for the influence of the fibers on the fluid motion to be neglected can be found in Tucker (1991).

When the mold filling of thin-wall parts is analyzed, as is the present case, the following two “lubrication” approximations are generally made: (a) through-the-thickness-variations in pressure are neglected and (b) the pressure field is taken to satisfy Hele-Shaw (elliptic) equation (Moldflow Plastics Insight, 2006). These approximations were used in the present work since they greatly simplify the effort needed to obtain the solution for the governing equations.

Mold-filling governing differential equations were subjected to the following boundary conditions in the present work: (a) either the inlet-flow rate or the pressure boundary conditions are defined at the injection points (gates); (b) a zero-pressure condition is defined on the advancing flow front; and (c) a zero-normal-pressure gradient is specified over the mold-cavity-surface. These conditions do not ensure a no-slip condition over the mold-cavity-surface, which may allow the fluid to “slip”. The resulting inaccuracies in the velocity-field predictions, however, were found not to be significant (Grujicic et al., in press; Guell and Lovalenti, 1995). Since the aforementioned lubrication approximations limit the analysis to the consideration of only the flow parallel with the local mid-plane, the approach used in the present work cannot be used to model the fountain flow (a flow type containing velocity components normal to the local mold wall). To reduce/eliminate the resulting inaccuracies in the temperature and the fiber-orientation predictions in the outermost layers of an injection molded part, the local approximation proposed in references Grujicic et al. (in press) and Crochet et al. (1994) was used in the present work.

To obtain temporal and spatial evolutions of the pressure during filling, the Hele-Shaw (elliptic) equation is solved numerically using the conventional Galerkin finite element method (within a local coordinate system in which the  $x_1$  axis coincides with a line connecting the first two nodes of a given element and the  $x_1$  and  $x_2$  axes define the

mid-plane). Four-node tetrahedron elements are used to discretize the plastic injection-molded subcomponent while two-node beam elements to model the runner system. Before element-based equations are assembled, a local-to-global coordinate transformation is applied to obtain a full three-dimensional computational model in the global coordinate system.

The flow front is tracked using the standard node-centered control-volume approach (Moldflow Plastics Insight, 2006). Within this approach, within each time increment, the flow rate into each node located on the flow front is calculated. This is used in conjunction with a given time step to determine if the control volume associated with the node in question is filled. If the control volume is filled, the flow front is advanced to the node in question. Otherwise, the flow front is not advanced.

To obtain spatial and temporal evolutions of temperature during mold filling (and packing), the energy conservation equation is solved numerically in such a way that the convection and viscous dissipation terms from a previous time step are treated as source terms during the current time step. Fast heat conduction over the metal stamping and mold surfaces is accounted for using a cycle-averaged (constant and uniform) temperature boundary condition at the U-shape/polymer and mold/polymer interfaces. The cycle-averaged temperature of the U-shape and mold surfaces is obtained by solving a three-dimensional steady-state heat conduction equation using a boundary element method (Grujicic et al., in press; Rezayat and Burton, 1990). The effect of thermal contact resistance at the metal-stamping/mold contact surfaces (which leads to higher plastic-melt temperatures) is obtained using the procedure proposed by Grujicic et al. (2005).

#### 2.4.2. Fiber orientation distribution analysis

For accurate predictions of the shrinkage and warping of an injection-molded part made of fiber-filled thermo-plastics, knowledge of the (flow-induced) fiber-orientation distribution throughout the part is critical (Grujicic et al., in press; Folgar and Tucker, 1984; Fan et al., 1998; Phan-Thien and Zheng, 1997). Since most commercial fiber-filled thermo-plastics commonly used for injection molding can be classified as semi- or highly concentrated suspensions, fiber/fiber interactions and spatial constraints to the fiber motion may significantly affect the final fiber-orientation distribution in the part.

Fiber/fiber interactions are accounted for, in the present work, using Folgar and Tucker model (Folgar and Tucker, 1984). In this model, A suspension-specific isotropic parameter,  $C_1$ , called the “Interaction Coefficient” is introduced in the diffusion term of the equation of motion for an isolated fiber in a Newtonian fluid originally proposed by Jeffery (Jeffery, 1922). The value for  $C_1$  is assessed using direct numerical-simulations of fiber/fiber interactions within simple-shear flow (Fan et al., 1998) in which short-range interactions are quantified using a lubrication model (Yamane et al., 1994) while long-range interactions were calculated using a boundary element method.

The orientation of a fiber is defined using the unit vector  $p$  which is collinear with the fiber axis. The fiber-orientation

probability-distribution function is then defined using the second,  $-a_{ij} = \langle pp \rangle$ , and the fourth,  $a_{ijkl} = \langle pppp \rangle$ , order orientation tensors, where the angular brackets denote the ensemble average. The temporal evolution of fiber orientation is defined by the Folgar-Tucker equation (Advani and Tucker, 1987). To solve this equation, the fourth-order tensor needs to be expressed in terms of the second-order tensor. The “closure approximation” proposed in Grujicic et al. (in press) and Doi (1981) is used in the present work. Following determination of the fiber orientation unit normal,  $p$  (as a function of the initial fiber orientation, aspect ratio, the number density in the suspension and the shear-strain magnitude), the components of the second- and fourth-order orientation tensors  $a_{ij}$  and  $a_{ijkl}$  are computed. These are next used in an anisotropic rotary diffusion equation to determine the magnitude of the fiber/fiber interaction coefficient  $C_1$ , and, in turn, the final fiber-orientation distribution.

The fiber-orientation distribution equation is solved numerically using the explicit Euler time-differencing scheme with a time step which is smaller than that used for the flow front advancement analysis and which satisfies the appropriate Courant stability criterion. For the fiber-orientation governing equation, the fiber-orientation tensors in the elements which are associated with the injection gates have to be specified. While the exact fibers orientations at the gates locations are usually unknown, the choice of the initial condition has been found to have little impact on the final orientation distribution of the fibers (Grujicic et al., in press; Zheng et al., 1999).

As mentioned earlier, the Hele-Shaw approximation does not include the effect of the lateral mold-walls on the advancement of flow field which, in turn, can lead to incorrect predictions of the fibers orientation in the outermost layers of an injection-molded part. This, consequently, may lead to incorrect prediction of the part warping. To overcome these shortcomings, two *ad hoc* remedies are used in the present work: (a) a vanishing tangential velocity along the mold walls is imposed during fiber-orientation calculations when computing velocity gradients from the velocity field; and (b) an “infinite-aspect-ratio” assumption is used for the fibers near the mold walls (Grujicic et al., in press; Lipscomb et al., 1988).

#### 2.4.3. Plastics material packing analysis

While the packing phase of the injection-molding process is governed by the same conservation equations as the filling phase, an additional equation, the equation of state (also known as the  $P$ - $V$ - $T$  relation), must be defined in order to include the effect of melt compressibility. The  $P$ - $V$ - $T$  relation defines a functional relationship between the specific volume,  $\hat{V}$ , temperature, pressure, and cooling rate.

A two-domain Tait  $P$ - $V$ - $T$  relation (Grujicic et al., in press; Moldflow Plastics Insight, 2006) was used in the present work. It should be noted that a number of material properties (such as volume thermal expansion coefficients and compressibility) and their temperature and pressure dependencies are derived from the equation of state. Also, the  $P$ - $V$ - $T$  relation is used to represent various phase transformations such as freezing/melting, crystallization, and ductile-to-glass transition.

## 2.5. Micro-mechanics analysis of the effective materials properties

As mentioned earlier, for injection molded thermo-plastics filled with fibers, isotropic material models are generally not valid unless the embedded fibers are randomly oriented. Typically, fiber-induced material anisotropy can have a profound influence on the extent and distribution of residual stresses and shrinkage/warping in injection molded parts. In the previous section, it was demonstrated how non-random orientation-distributions of the fibers are induced by the melt-flow kinematics during filling and, to a lesser extent during packing. In this section, the development/utilization of a micromechanical model which can be used to estimate anisotropic elastic and thermal properties of a fiber-filled/thermo-plastic-matrix composite from the properties of the constituent fiber and matrix materials and the known fiber-orientation distribution was discussed (Papathanasiou and Guell, 1997).

Materials processed using injection molding are generally considered to be transversely isotropic, i.e. their properties are equal in two directions (the transverse direction and through-the-thickness direction). The elastic response of such materials is defined by five (temperature-dependent) elastic moduli: the longitudinal Young's modulus  $E_{11}$ , the transverse Young's modulus  $E_{11}$ , the in-plane shear modulus  $G_{12}$ , the out-plane shear modulus  $G_{23}$ , and the plane-strain bulk modulus  $K_{23}$ . The Poisson's ratios  $\nu_{12}$ ,  $\nu_{21}$  and  $\nu_{23}$  can, in turn, be determined from these elastic moduli using standard relations (e.g. Zheng et al., 1999). These properties are defined with respect to a local coordinate system in which the 1 direction is taken to coincide with the fiber axis and to be normal to the plane of isotropy (defined by the 2 and 3 directions).

The elastic and thermal properties of short-fiber filled thermoplastics are typically assessed using a two-step micro-mechanics procedure. First, the properties of the corresponding material in which the fibers are fully aligned in one direction are assessed. Next, an orientation averaging procedure is applied to include the effect of the actual fiber-orientation distribution at hand.

**Step 1:** Derivations of the properties of materials in which the fibers are fully aligned can be found in many sources (e.g. Papathanasiou and Guell, 1997). Thermo-elastic properties of injection-molded fiber-filled polymers are typically specified as longitudinal,  $\alpha_1$ , and transverse,  $\alpha_2$ , thermal expansion coefficients and are defined in terms of the thermal expansion coefficients for the fiber and the matrix as (Schapery, 1968):

$$\alpha_1 = \frac{E_f \alpha_f \phi + E_m \alpha_m (1 - \phi)}{E_f \phi + E_m (1 - \phi)} \quad (1)$$

and

$$\alpha_2 = (1 + \nu_m) \alpha_m (1 - \phi) + (1 + \nu_f) \alpha_f \phi - \alpha_1 \nu_{12} \quad (2)$$

where subscripts f and m denote fiber and matrix, respectively,  $\phi$  the fiber volume fraction,  $E$  the Young's modulus and  $\nu$  is the Poisson ratio.

**Step 2:** For a transversely isotropic material with the isotropy-plane normal coinciding with the 1 direction, the fol-

lowing form of Hooke's law holds:

$$\begin{pmatrix} \sigma_1 \\ \sigma_2 \\ \sigma_3 \\ \sigma_4 \\ \sigma_5 \\ \sigma_6 \end{pmatrix} = \begin{pmatrix} c_{11}^{(e)} & c_{12}^{(e)} & c_{12}^{(e)} & 0 & 0 & 0 \\ c_{12}^{(e)} & c_{22}^{(e)} & c_{23}^{(e)} & 0 & 0 & 0 \\ c_{12}^{(e)} & c_{23}^{(e)} & c_{22}^{(e)} & 0 & 0 & 0 \\ 0 & 0 & 0 & c_{44}^{(e)} & 0 & 0 \\ 0 & 0 & 0 & 0 & c_{55}^{(e)} & 0 \\ 0 & 0 & 0 & 0 & 0 & c_{66}^{(e)} \end{pmatrix} \begin{pmatrix} \varepsilon_1 \\ \varepsilon_2 \\ \varepsilon_3 \\ \varepsilon_4 \\ \varepsilon_5 \\ \varepsilon_6 \end{pmatrix} \quad (3)$$

in which  $c_{44}^{(e)} = (1/2)(c_{22}^{(e)} - c_{23}^{(e)})$ ,  $c_{55}^{(e)} = c_{66}^{(e)}$  and the contracted notation (1 = 11, 2 = 22, 3 = 33, 4 = 23, 5 = 13 and 6 = 12) is used.

The components of the elastic-stiffness matrix are defined in terms of the elastic moduli as (Halpin and Kardos, 1976):

$$c_{11}^{(e)} = \frac{(1 - \nu_{23})E_{11}}{1 - \nu_{23} - 2\nu_{12}\nu_{21}} \quad (4)$$

$$c_{12}^{(e)} = \frac{\nu_{23}E_{11}}{1 - \nu_{23} - 2\nu_{12}\nu_{21}} \quad (5)$$

$$c_{22}^{(e)} = \frac{E_{22}}{2(1 - \nu_{23} - 2\nu_{12}\nu_{21})} + G_{23} \quad (6)$$

$$c_{23}^{(e)} = \frac{E_{22}}{2(1 - \nu_{23} - 2\nu_{12}\nu_{21})} - G_{23} \quad (7)$$

$$c_{55}^{(e)} = G_{12} \quad (8)$$

Once the properties of short-fiber uni-directionally reinforced polymers are determined, an orientation averaging procedure is used in conjunction with the known fibers orientation tensors to determine the corresponding assembly-average elastic and thermo-elastic material properties as (Advani and Tucker, 1987):

$$\begin{aligned} \langle c_{ijkl}^{(e)} \rangle &= B_1 a_{ijkl} + B_2 (a_{ij} \delta_{kl} + a_{kl} \delta_{ij}) + B_3 (a_{ik} \delta_{jl} + a_{il} \delta_{jk} + a_{jl} \delta_{ik} + a_{jk} \delta_{il}) \\ &\quad + B_4 \delta_{ij} \delta_{kl} + B_5 (\delta_{ik} \delta_{jl} + \delta_{il} \delta_{jk}) \end{aligned} \quad (9)$$

and

$$\langle \alpha_{ij} \rangle = (\alpha_1 - \alpha_2) a_{ij} + \alpha_2 \delta_{ij} \quad (10)$$

where  $B_i$ 's denote the five invariants of the stiffness tensor of the uni-directionally reinforced polymers (Advani and Tucker, 1987). It should be noted that the expressions given in Eqs. (9) and (10) are specific examples of the so-called "effective material-properties averaging schemes". Within such schemes, a composite material is considered as an aggregate of discrete constituent materials and different averaging schemes are based on different assumptions. For example, the thermal expansion coefficient defined by Eq. (10) is obtained under the assumption of a uniform stress and temperature gradient throughout the fiber/matrix aggregate (Camacho et al., 1990; Eduljee et al., 1994).

2.6. In-mold stress development and distribution analysis

There are two main sources for residual stresses in injection molded parts: (a) visco-elastic deformations of the thermoplastic material during mold-filling and material-packing stages can give rise to the development of the so-called “flow-induced” residual stresses and (b) when the (inhomogeneous) cooling- and solidification-induced shrinkage of the polymer is restricted by the mold and metal-stamping(s) and the applied packing pressure, the so-called “thermally and pressure-induced” stresses are generated. Following the general practice, the flow-induced residual stresses are neglected in the present work, since these are readily relieved while the part resides in the mold at high temperatures prior to ejection. There are numerous reports of numerical investigations of the pressure and thermally induced stresses in injection molded parts in the literature (e.g. Bushko and Stokes, 1996). These investigations clearly revealed the effects of mold constraints and thermo-plastics material models on the extent and distribution of the residual stresses. However, there are no reports in the open literature addressing the effect of plastics/mold and/or plastics/metallic-stamping(s) adhesion on the development and the extent of residual stresses.

As discussed earlier, adhesion between the plastics and metal (tools and stampings) merely alters the boundary conditions in the in-mold stress analysis. Consequently, and considering the fact that a fairly detail description of the in-mold stress development analysis was presented in our recent work (Grujicic et al., in press), only a brief overview of the same will be given in the remainder of this section.

2.6.1. Anisotropic linear thermo-visco-elastic material formulation

As the injected material begins to cool inside the mold, its relaxation time starts to increase and approach the in-mold resident time. Hence, an accurate prediction of the thermal stresses entails the knowledge of the visco-elastic material properties. In the range of small strains, as is the present case, the visco-elastic behavior of an injection-molded fiber-filled thermo-plastics can be described using the anisotropic linear thermo-visco-elasticity (Bird et al., 1987; Tanner, 1988) in the form:

$$\sigma_{ij} = \int_0^t c_{ijkl}(\xi(t) - \xi(t')) \left( \frac{\partial \epsilon_{kl}}{\partial t'} - \alpha_{kl} \frac{\partial T}{\partial t} \right) dt' \tag{11}$$

where  $c_{ijkl}(t)$  is the fourth-order visco-elastic relaxation tensor and  $\xi(t)$  denotes the so-called “pseudo-time scale” defined by

$$\xi(t) = \int_0^t \frac{1}{a_T} dt' \tag{12}$$

where  $a_T$  is the time–temperature shift factor that reflects the inter-changeable effects of time and temperature on the material response. For amorphous polymers, the time-temperature shift factor in a temperature range between  $T_g$  and  $T_g + 100\text{K}$  (where  $T_g$  is the glass transition temperature) is generally

defined by the so-called WLF equation (Ferry, 1980) in the form:

$$\log_{10} a_T = - \frac{C_1(T - T_r)}{C_2 + (T - T_r)} \tag{13}$$

where  $C_1$  and  $C_2$  are constants and  $T_r$  is a reference temperature (the temperature at which elements of the fourth-order visco-elastic relaxation tensor are specified). When the relevant experimental data are lacking for a given material and the values for constants  $C_1$ ,  $C_2$  and  $T_r$ , cannot be assessed, the so-called “universal values”  $C_1 = 17.44$ ,  $C_2 = 51.6$ ,  $T_r = T_g$  are used.

For temperatures outside the above range or for semi-crystalline materials, the following Arrhenius-type expression is generally used to assess the time-temperature shift factor:

$$\ln a_T = \frac{E_a}{R} \left( \frac{1}{T} - \frac{1}{T_r} \right) \tag{14}$$

where  $E_a$  is the activation energy and  $R$  is the universal gas constant.

Materials obeying the time-temperature superposition principle are generally referred to as thermo-rheologically simple materials. In such materials, visco-elastic material functions determined at one temperature and plotted against the logarithmic time remain essentially unaltered when the temperature is changed. While fiber-filled thermo-plastics generally behave as rheologically complex materials, the material used in the present work is treated as being rheologically simple due to a lack of experimental data needed to evaluate the necessary parameters.

2.6.2. Definition of the in-mold stresses

To compute the in-mold stresses, the following procedure is utilized. First, the total-stress second-order tensor in Eq. (11) is decomposed into the hydrostatic stress and the deviatoric stress as

$$\sigma = -p_h I + \tau \tag{15}$$

where  $p_h$  is the hydrostatic pressure,  $I$  the second-order identity tensor and  $\tau$  is the deviatoric stress tensor. The hydrostatic pressure is next defined as

$$p_h = -\frac{1}{3} \sigma_{ii} = \int_0^t \left( \beta \frac{\partial T}{\partial t'} - K T r \dot{\epsilon} \right) \tag{16}$$

where  $\beta$  and  $K$  are given in terms of the elastic constants  $c_{ij}$  and thermal  $\alpha_i$  material properties (using the contracted notation) as

$$\beta = \frac{1}{3} [(c_{11}^{(e)} + c_{12}^{(e)} + c_{13}^{(e)})\alpha_1 + (c_{12}^{(e)} + c_{22}^{(e)} + c_{23}^{(e)})\alpha_2 + (c_{13}^{(e)} + c_{23}^{(e)} + c_{33}^{(e)})\alpha_3] \tag{17}$$

and

$$K = \frac{1}{3} (c_{13}^{(e)} + c_{23}^{(e)} + c_{33}^{(e)}) \tag{18}$$

As mentioned earlier, in injection molded parts, the (predominant) fiber direction is chosen as the material 1 direction while

the material 3 direction is aligned with the corresponding through-the-thickness direction.

The normal components of the deviatoric stress are next defined as

$$\tau_{ii}(t) = 2 \int_0^t G_i(\xi(t) - \xi(t')) \frac{\partial \varepsilon_{ii}^d}{\partial t} dt' - \int_0^t \beta_i(\xi(t) - \xi(t')) \frac{\partial T}{\partial t} dt' \quad (19)$$

where  $ii = 11, 22, 33$ ,  $i = 1, 2, 3$ ,  $\varepsilon_{ij}^d$  is the deviatoric strain defined as

$$\varepsilon_{ij}^d = \varepsilon_{ij} - \frac{1}{3} \text{Tr} \varepsilon \delta_{ij} \quad (20)$$

$$G_i(t) = G_i(0)F(t) \quad (i = 1, 2, 3) \quad (21)$$

and

$$\beta_i(t) = \beta_i(0)F(t) \quad (i = 1, 2, 3) \quad (22)$$

with

$$G_1(0) = \frac{1}{2} (c_{23}^{(e)} - c_{13}^{(e)} + c_{33}^{(e)}) \quad (23)$$

$$\begin{aligned} \beta_1(0) = & \frac{1}{3} [(2c_{11}^{(e)} - c_{12}^{(e)} - c_{13}^{(e)})\alpha_1 + (2c_{12}^{(e)} - c_{22}^{(e)} - c_{23}^{(e)})\alpha_2 \\ & + (2c_{13}^{(e)} - c_{23}^{(e)} - c_{33}^{(e)})\alpha_3] \end{aligned} \quad (24)$$

and  $G_2(0)$ ,  $G_3(0)$ ,  $\beta_1(0)$  and  $\beta_2(0)$  are defined using analogous expressions and it is assumed that all  $G_i(t)$  and  $\beta_i(t)$  depend on the same relaxation function  $F(t)$ .

The relaxation function is approximated as a sum of weighted exponential (the so-called *Prony series*) functions as

$$F(t) = \sum_{k=1}^N g_k \exp\left(-\frac{t}{\lambda_k}\right) \quad (25)$$

with  $\sum_{k=1}^N g_k = 1$ . The current model for  $F(t)$  thus requires the knowledge of  $N$  ( $g_k, \lambda_k$ ) pairs of values.

The off-diagonal components of the deviatoric stress are next computed using a procedure which is analogous to the aforementioned one used for the computation of the normal components of the deviatoric stress.

### 2.6.3. Boundary conditions

In the absence of adhesion, the following boundary conditions are generally specified:

1. When the part resides in the mold and the injected material contains both a solid outer-layer and a liquid core, the normal stress  $\sigma_{33}$  is set equal to the negative fluid pressure,  $\sigma_{33} = -p$ . In addition, all strain components except for  $\varepsilon_{33}$  are set to zero (in other words, the part is considered to be constrained within its mid-plane);
2. When the part resides in the mold and the injected material has completely solidified, the part may either be in contact with the metal-stamping/mold or be detached from it. In the first case,  $\sigma_{33}$  is determined using the condition:

$\int_{-h/2}^{h/2} \varepsilon_{33} dx_3 = 0$ . In the latter case,  $\sigma_{33} = 0$ . Again, all strain components except for  $\varepsilon_{33}$  are set to zero.

3. After the part is ejected from the mold, no external loads are applied to it and, hence,  $\sigma_{33}$  is determined from the following zero-surface-traction boundary condition:  $\sigma_{ij}n_j = 0$ , where  $n_j$  is the  $j$ th component of the plastics-subcomponent outward-surface unit normal (except for the plastics surfaces which are in contact with the metal-stamping).

When adhesion is present at the metal/plastics interfaces, on the other hand, no boundary conditions are applied to the plastics over such interfaces. Instead, the interactions between the plastics and the metal are directly modeled through the use of interfacial adhesion finite elements, [Appendix A](#).

### 2.6.4. Numerical procedures

A detailed account of the numerical procedure used to compute the evolution of in-mold stresses can be found in our recent work ([Grujicic et al., in press](#)). The procedure is of an incremental and discrete type and is based on the known stress state at the previous time step. In the same reference, a detailed account of a procedure used for the calculation of the incremental strains is also presented.

### 2.6.5. Post-ejection shrinkage and warping analyses

While the injection-molded PMH component resides in the mold, it is constrained and cannot distort. However, after ejection, the component can undergo shrinkage and warping. In the present case, the injected plastics remains somewhat constrained by its adhesion to the metal stamping. As mentioned earlier, shrinkage and warping analyses were carried out using ABAQUS/Standard. In such analyses, the same finite element mesh is utilized as that used in the filling and packing analyses, except that a set of interfacial cohesion elements is added to model explicitly the effect of adhesion at the plastics/metal interfaces.

When no adhesion is considered at the metal-stamping/thermoplastics and mold/thermoplastics interface, the in-mold residual stresses can be calculated using the “Stress” module of Moldflow Plastics Insight. In that case, the computed in-mold residual stresses, as well as temperatures and element-based through-the-thickness variations in thermo-mechanical properties of the injected thermoplastic material are exported from Moldflow Plastics Insight to ABAQUS/Standard. The exported residual stresses and temperatures are then used to define the initial conditions in the PMH component right after its ejection and, in turn, to construct the loading term in the coupled thermo-mechanical finite element equations. Next, a boundary condition is applied by constraining all six degrees of freedom for a single node of the metal stamping in order to prevent the PMH component from undergoing a rigid body motion. Also, free convection boundary conditions are prescribed on all free surfaces. Furthermore, since the ejected PMH component spends some amount of time at the temperature at which thermoplastics exhibit viscous behavior, a linear visco-elastic residual-stress and warping finite element analysis is performed in the present work.

When adhesion at the metal-stamping/thermoplastics and mold/thermoplastics interfaces is taken into account, the in-mold residual stresses had to be calculated using ABAQUS/Standard since Moldflow does not allow consideration of adhesion. In this case, temperatures and element-based through-the-thickness variations in thermo-mechanical properties of the injected thermoplastic material at the end of the packing stage are exported from Moldflow to ABAQUS/Standard. In this case, development of the in-mold stresses and the post-ejection shrinkage and warping of the PMH component are carried out in ABAQUS/Standard. The procedure is essentially identical to the one described above with an exception that the metal-stamping/thermoplastics boundaries are treated as adhesion-bonded interfaces rather than contact surfaces.

### 3. Results and discussion

In this section, selected injection-molding simulation and thermo-mechanical finite-element analysis results are presented and discussed. As explained earlier, the main objective of the present work was the assessment of the contribution that metal-stamping/plastics-subcomponent adhesion makes

to the development of residual stresses and to warping in the DA-PMH components. Residual stresses can play a key role in limiting durability of such components while warping can have negative consequences to the assembly process (as well as on the component durability).

#### 3.1. Injection mold-filling and material-packing analyses

An example of the typical mold-filling/material-packing results obtained using Moldflow is shown in Fig. 4(a) and (b). In Fig. 4(a), a contour plot of the filling time is shown along with the symbols (elongated cones) for the injection ports. In Fig. 4(b), on the other hand, the orientation of the fibers is depicted using a contour plot for the probability that the fiber axis is aligned with the local principal direction 1 (defined as the local direction connecting nodes 1 and 2). As mentioned earlier, the orientation of the fibers affects the extent of orthogonality in the mechanical and thermal properties of the injection-molded fiber-reinforced polymer.

The main findings based on the results displayed in Fig. 4(a) and (b) (and the other mold-filling/material-packing results which are not shown for brevity), can be summarized as follows:

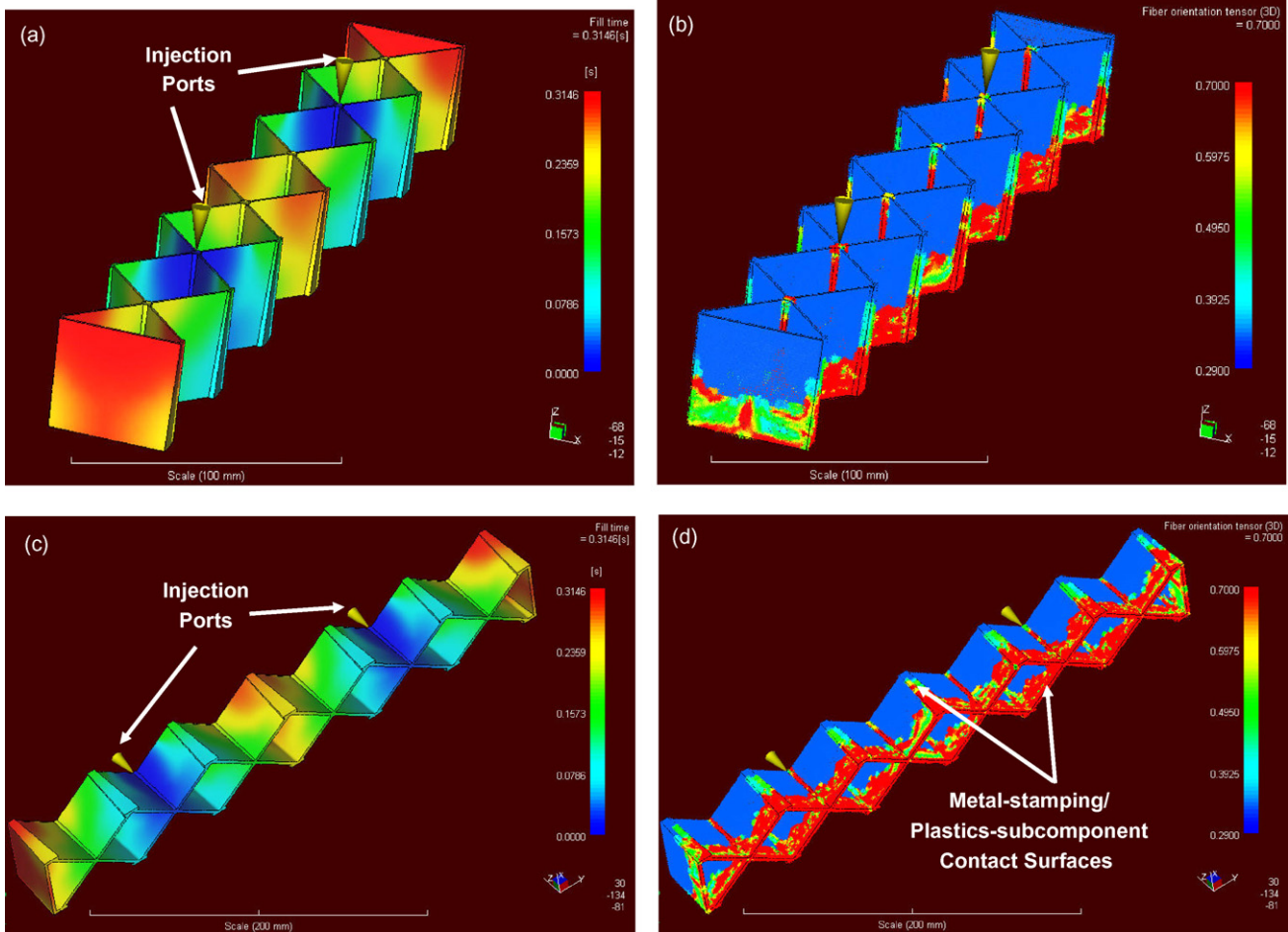


**Fig. 4 – Injection-molding simulation results pertaining to: (a) the mold-fill time and (b) fiber-orientation probability function (please see text for details). The results displayed in (c) and (d) correspond respectively to those displayed in (a) and (b), but involve a different view angle.**

- (a) Due to a symmetric placement of the two injection ports, Fig. 4(a), melt-flow is fairly balanced (i.e. the sections of the mold which are filled last, are filled at approximately the same time). This finding suggests that no portion of the injection-molded plastic subcomponent will be over-packed and that a fairly uniform distribution of the thermoplastics density will be attained minimizing the tendency for post-ejection PMH-component warping;
- (b) A detailed analysis of the results displayed in Fig. 4(b) and the results pertaining to the melt-flow directions at the end of the material-packing stage indicates that fibers are fairly well aligned with the local flow direction imparting a large extent of orthotropy to the injection-molded short glass-fiber reinforced nylon 6; and
- (c) A fairly uniform distribution of the temperature within the injection-molded thermoplastic subcomponent is found at the end of the packing stage (the results not shown for brevity). This temperature is, at the most, only few tenths of a degree lower than the melt temperature. This finding is consistent with the fact that the mold-fill time, Fig. 4(a), is only ca. 0.3 s.

### 3.2. Thermo-mechanical analysis of residual stresses and warping in direct-adhesion PMH components

As explained earlier, when adhesion at the metal-stamping/plastic-subcomponent contact surfaces is not considered, the in-mold residual stresses may develop as a result of the con-

straints imposed by the stamping and the mold onto the plastics subcomponents as it undergoes thermal and solidification shrinkage. Under such conditions, thermoplastic subcomponent is free to detach itself from the metal-stamping (and the mold), in the subcomponent through-the-thickness direction. When adhesion is present at the metal-stamping/thermoplastic-subcomponent interfaces, thermoplastic is constrained from freely detaching from the metal-stamping surface. This provides an additional source of in-mold stresses (and, in turn, of the residual stresses in the PMH component).

An example of the results obtained in the present thermo-mechanical analysis which clearly revealed the effect of metal-stamping/thermoplastic-subcomponent adhesion is presented in Figs. 5–8. The spatial-distribution results for the von Mises equivalent stress corresponding to the “no-adhesion” case are presented in Fig. 5(a) while their counterparts referring to the case when adhesion is taken into account are displayed in Fig. 5(b). The results displayed in Fig. 5(a) and (b) clearly reveal two important consequences arising from adhesion at the metal-stamping/plastics-subcomponent contact surfaces: (a) the overall level of the (residual) von Mises stresses is significantly increased and (b) such stresses are more localized in the regions of direct contact between the metal stamping and the plastics subcomponent.

A comparison of the maximum principal elastic strain results obtained in the “no-adhesion” and “adhesion” cases is displayed in Fig. 6(a) and (b), respectively. The extent of the

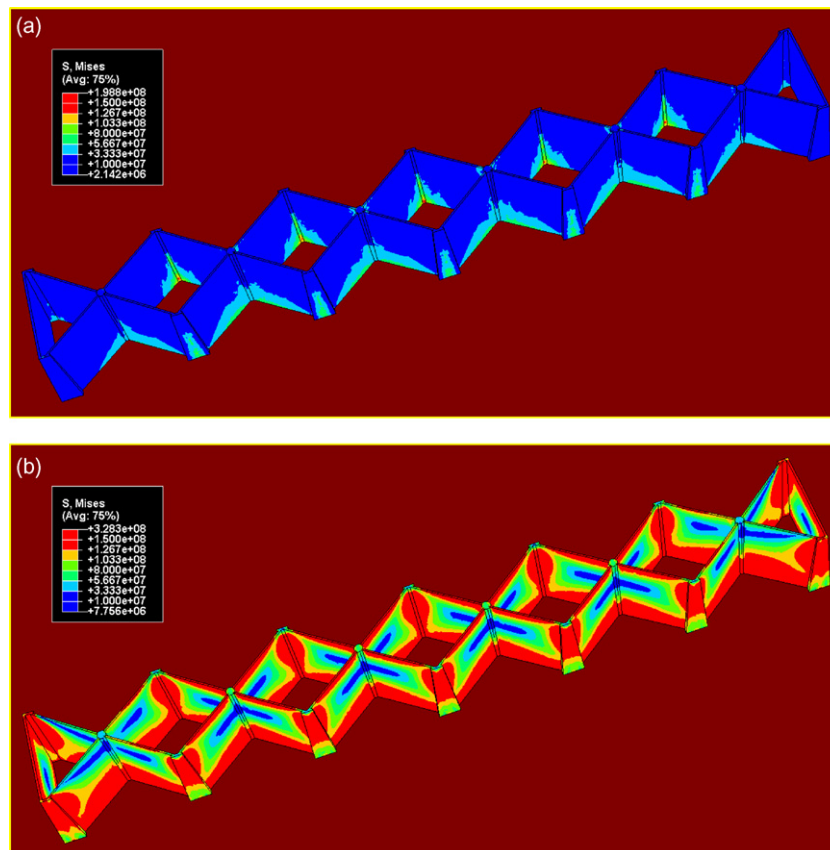
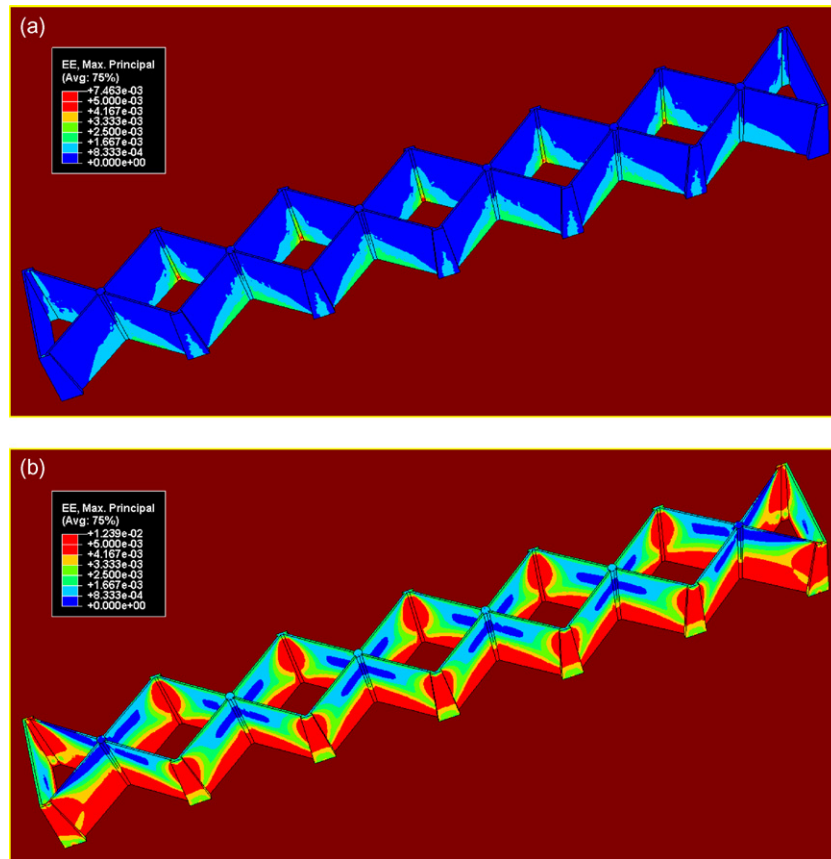


Fig. 5 – Distribution of the von Mises equivalent stress in the plastics subcomponent in the: (a) absence and (b) presence of adhesion at the metal-stamping/plastics-subcomponent interface.



**Fig. 6 – Distribution of the maximum principal elastic strain in the plastics subcomponent in the: (a) absence and (b) presence of adhesion at the metal-stamping/plastics-subcomponent interface.**

elastic strains in the thermoplastic component in the adhesion case is clearly significantly higher, particularly in the metal-stamping/plastics-subcomponent interfacial regions. This finding is consistent with the fact that the plastics subcomponent is constrained from freely contracting during cooling and solidification and, hence, experiences tensile elastic deformations. This point is further reinforced in Fig. 7(a) and (b) where a comparison is made of the normal  $zz$  component of the elastic strain results obtained in the “no-adhesion” and “adhesion” cases. The  $zz$  component of the strain is selected since it has the same (upward) orientation for all the elements in the plastics subcomponent. It should be noted that only the plastics subcomponent was displayed in Figs. 5–7.

The extent of warpage in the PMH component in the “no-adhesion” and the “adhesion” cases is displayed in Fig. 8(a) and (b), respectively. For clarity, only the metal-stamping is shown in the two cases. It should be noted that in order to magnify the effect of warpage on the component shape, a nodal-displacement scale factor of 10 is applied. It is clear that the extent of warpage (even though relatively small) is higher in the “adhesion” case, where, thermal and solidification shrinkage of the plastics subcomponent is transferred to the metal stamping via metal-stamping/plastics-subcomponent adhesion bonding. As discussed earlier, PMH component warpage can have deleterious effects on the assembly process (i.e. some preloading may have to be applied to the component to make

if fit) and on the component durability (i.e. a sustained loading is put into the component contribution to an earlier onset of damage and potential failure).

Under the injection-molding process conditions used to generate the results presented in Figs. 5–8, no evidence of decohesion at the metal-stamping/polymer-subcomponent interfaces was observed. This is exemplified in the  $x$ - $y$  plot in Fig. 9 (curve A), in which the maximum normal interfacial-displacement discontinuity (at an arbitrarily selected location) never exceeds the critical normal (decohesion initiation) separation (10 nm). To show that under different injection-molding process conditions, interfacial decohesion may take place, normal interfacial displacement discontinuity results correspond to the case of a more aggressive cooling are also shown in Fig. 9 (curve B). In this case, it is seen that decohesion has occurred and, at the location in question, no load transfer (in tension or shear) can take place between the plastics subcomponent and the metal stamping. This finding is quite significant since faster cooling is attractive due to the resulting shorter cycle time. The present results show, however, that in an attempt to reduce the cycle time, one may compromise the integrity of the DA-PMH component by creating defective plastics-subcomponent/metal-stamping adhesion-bonded interfaces.

It should be noted that all the thermo-mechanical calculations of the in-mold/residual stresses and the PMH-component warpage development were carried out using

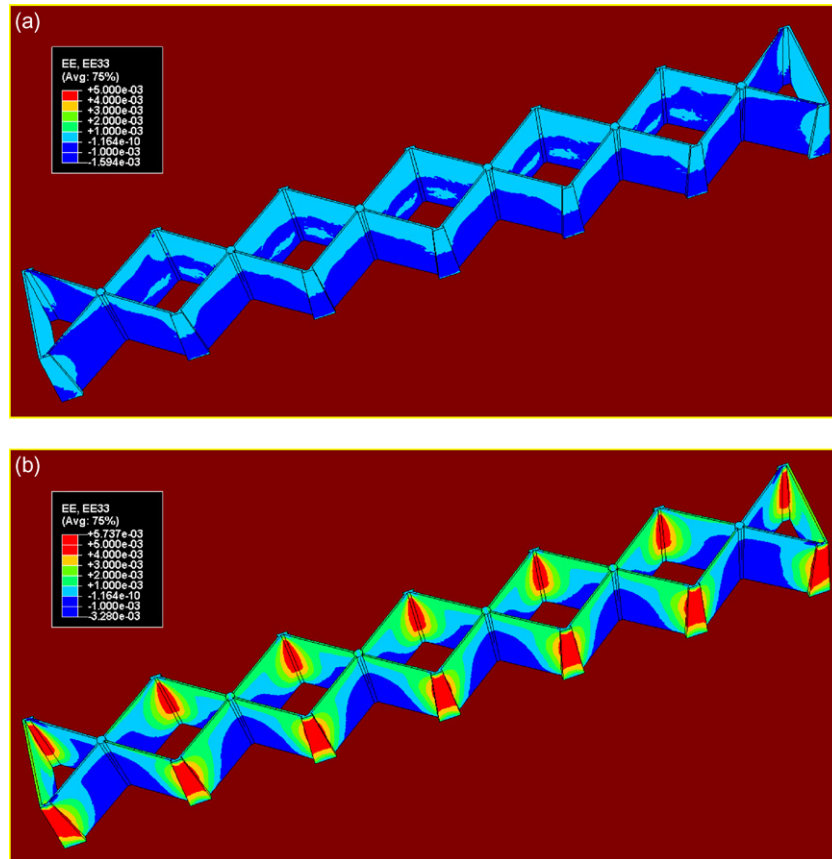


Fig. 7 – Distribution of the zz-component of the elastic strain in the plastics subcomponent in the: (a) absence and (b) presence of adhesion at the metal-stamping/plastics-subcomponent interface.

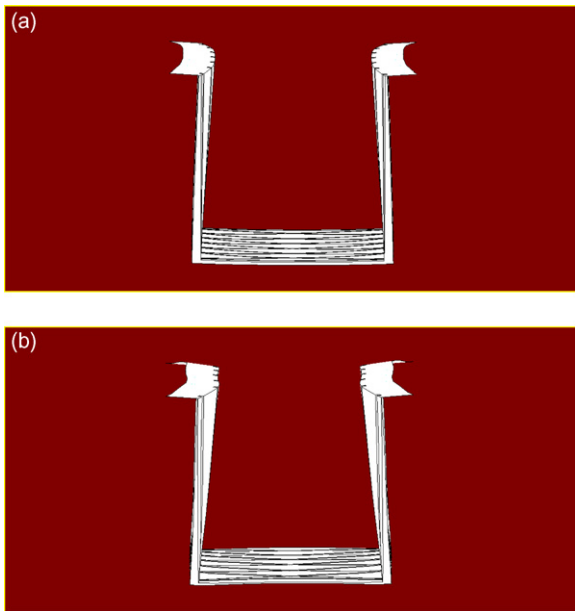
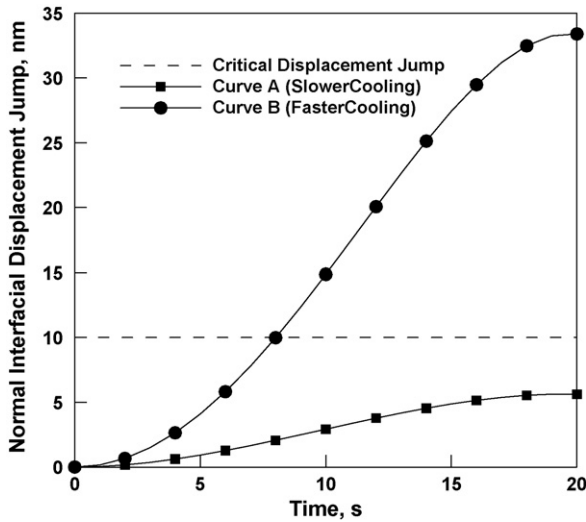


Fig. 8 – A comparison of the extents of warping in the metal-stamping in the: (a) absence and (b) presence of adhesion at the metal-stamping/plastics-subcomponent interface.

Abaqus/Standard computer program. It is well-established that such calculations accurately capture the basic behavior and trends. However, a highly comprehensive analysis (involving over 20,000 injection moldings each with varied process conditions, thickness and material) carried out by Moldflow Inc. (Moldflow Plastics Insight, 2006) revealed that the warpage predictions, based solely on thermo-mechanical computational analyses are sufficiently accurate (within 20%) in only about 15–20% of the cases. To overcome this problem, the so-called CRIMS (Corrected In-mold Residual Stress) technique is implemented in Moldflow. CRIMS is a hybrid technique which utilizes measured shrinkage data to correct/improve the in-mold/residual stress and warpage development predictions made by the thermo-elastic computational analyses. By comparing the computational predictions with the experimentally measured shrinkages, a set of CRIMS correction functions has been created and the function coefficients stored in the Moldflow Material Database. When an in-mold/residual stress and warping analysis is carried out using Moldflow, these coefficients are used to correct the computational results. This procedure was utilized in our previous work (Grujicic et al., in press) in which no effect of metal-stamping/plastics-subcomponent adhesion was investigated. Unfortunately, in its present formulation, Moldflow does not allow the inclusion of adhesion effects. Consequently, all the thermo-mechanical analyses had to be done outside Moldflow, using Abaqus Standard. Since the CRIMS technique is not implemented in



**Fig. 9 – The effect of cooling rate on the onset of adhesion at the metal-stamping/polymer-subcomponent contact surfaces. The critical value of the interfacial displacement jump corresponds to the onset of normal-mode decohesion.**

Abaqus/Standard, the in-mold/residual stress and warping corrections discussed above cannot be applied. Furthermore, in the absence of the corresponding experimental data, the results displayed in Fig. 5(a) and (b) should be considered only as indicators for physical trends and less significance should be given to their quantitative nature. Nevertheless, the results displayed in Fig. 5(a) and (b), clearly reveal that adhesion may play an important role and should be taken into account when DA-PMH components are designed and their manufacturing process specified.

Since the direct-adhesion PMH technology is quite new, there is very limited amount of experimental data reported in the open literature. This fact and the fact that the on-going work carried out by the authors is of purely computational nature, prevents a direct validation of the results obtained in the present work. Nevertheless, the results obtained in the present work are consistent with the general expectations one can have regarding the effect of polymer-to-metal adhesion onto the changes in the magnitude and the distribution of in-mold and post-ejection residual stresses in DA-PMH components.

#### 4. Summary and conclusions

Based on the results obtained in the present work, the following main summary remarks and conclusions can be drawn:

1. Injection-molding simulations are combined with thermo-mechanical finite element analysis to assess the role of adhesion at the metal-stamping/plastic-subcomponent coated surfaces in the development of in-mold/residual stresses and warping in direct-adhesion polymer metal hybrid components.
2. Adhesion at the metal-stamping/plastic-subcomponent interfaces is modeled using a cohesive-zone formula-

tion within which a special set of interfacial elements is used whose mechanical constitutive response is defined using appropriate normal and shear traction vs. interfacial-displacement discontinuity laws.

3. In general, adhesion at the metal-stamping/plastic sub-component interfaces has been found to increase both the magnitude of residual stresses and the extent of PMH component warping. Both of these effects can have negative consequences on the assembly process and the component durability and must be considered when a DA-PMH component is and its manufacturing process are designed.

#### Acknowledgements

The material presented in this paper is based on work conducted as a part of the project “Lightweight Engineering: Hybrid Structures: Application of Metal/Polymer Hybrid Materials in Load-bearing Automotive Structures” supported by BMW AG, München, Germany. The authors are indebted to Drs. David Angstadt, Greg Moco and Lonny Thomson for stimulating discussions.

#### Appendix A. Polymer/metal decohesion/de-bonding potential and its

The plastics/metal interfaces have been modeled in the present work using the “cohesive zone framework” originally proposed by Needleman (1987). The cohesive zone is assumed to have a negligible thickness when compared with other characteristic lengths of the problem, such as the plastics-wall thickness, the width of metal-stamping grooves, or the characteristic lengths associated with the stress/strain gradients. The mechanical behavior of the cohesive zone is characterized by a traction–displacement relation, which is introduced through the definition of an *interfacial potential*,  $\psi$ . The perfectly bonded plastic/metal interface is assumed to be in a stable equilibrium, in which case the potential  $\psi$  has a minimum and all tractions vanish. For any other configuration, the value of the potential is taken to depend only on the displacements discontinuities (jumps) across the interface. To simplify the analysis presented in this section and reduce the length of the document, a two-dimensional case is treated. The plastics/metal decohesion analysis used in this paper was, however, a full three-dimensional analysis.

For a two-dimensional problem, the interface displacement jump (i.e. the interfacial separation) is expressed in terms of its normal component,  $U_n$ , and a tangential component,  $U_t$ , where both components lie in the  $x$ - $y$  plane of the Cartesian coordinate system. Differentiating the interface potential function  $\psi = \hat{\psi}(U_n, U_t)$  with respect to  $U_n$  and  $U_t$  yields respectively, the normal and tangential components of  $F$ , the traction per unit plastic/metal interface area in the deformed configuration, as

$$F_n(U_n, U_t) = \frac{-\partial \hat{\psi}(U_n, U_t)}{\partial U_n} \tag{A1}$$

$$F_t(U_n, U_t) = \frac{-\partial \hat{\psi}(U_n, U_t)}{\partial U_t} \quad (\text{A2})$$

The interface traction/separation constitutive relations are thus fully defined by specifying the form for the interface potential function  $\hat{\psi}(U_n, U_t)$ . The interface potential of the following form initially proposed by Socrate (1995) is used in the present study:

$$\hat{\psi}(U_n, U_t) = \left\{ -e\sigma_{\max}\delta_n + \frac{1}{2}\tau_{\max}\delta_t \log \left[ \cosh \left( 2\frac{U_t}{\delta_t} \right) \right] \right\} \times \left[ e^{-U_n/\delta_n} \left( 1 + \frac{U_n}{\delta_n} \right) \right] \quad (\text{A3})$$

where the parameters  $\sigma_{\max}$  and  $\tau_{\max}$  are, respectively, the normal and tangential interfacial (cohesion) strengths, and  $\delta_n$  and  $\delta_t$  are the corresponding characteristic interface (separation/sliding) lengths. Differentiation of Eq. (A3) with respect to  $U_n$  and  $U_t$  yields the following expressions for the normal and tangential interfacial tractions:

$$F_n(U_n, U_t) = \left\{ e\sigma_{\max} - \frac{1}{2}\tau_{\max}\frac{\delta_t}{\delta_n} \log \left[ \cosh \left( 2\frac{U_t}{\delta_t} \right) \right] \right\} \times \left[ \frac{U_n}{\delta_n} e^{-U_n/\delta_n} \right] \quad (\text{A4})$$

$$F_t(U_n, U_t) = \left[ \tau_{\max} \tanh \left( 2\frac{U_t}{\delta_t} \right) \right] \left[ e^{-U_n/\delta_n} \left( 1 + \frac{U_n}{\delta_n} \right) \right] \quad (\text{A5})$$

Graphical representations of the two functions defined by Eqs. (A4) and (A5) are given in Fig. A1(a) and (b), respectively. If  $F_n$  given by Eq. (A4), is expressed for the case of purely normal interface decohesion, and the  $F_t$  for the case of pure sliding, one obtains:

$$F_n(U_n, U_t = 0) = F_n^0(U_n) = e\sigma_{\max} \left( \frac{U_n}{\delta_n} e^{-U_n/\delta_n} \right) \quad (\text{A6})$$

$$F_t(U_n = 0, U_t) = F_t^0(U_t) = \tau_{\max} \tanh \left( 2\frac{U_t}{\delta_t} \right) \quad (\text{A7})$$

An inspection of Eqs. (A6) and (A7) shows that the plastics/metal interface behavior is characterized by four parameters:  $\sigma_{\max}$ ,  $\delta_n$ ,  $\tau_{\max}$  and  $\delta_t$ ; where  $\sigma_{\max}$  is the peak normal traction for purely normal interface decohesion (i.e. the normal decohesion strength);  $\delta_n$  is the normal interface separation which corresponds to this peak traction;  $\tau_{\max}$  is an asymptotic shear traction for interface sliding (i.e. the shear decohesion strength); and  $\delta_t$  is a characteristic length in pure sliding, which corresponds to a shear traction 1% lower than  $\tau_{\max}$ , i.e.  $F_t^0(\delta_t) \approx 0.99 \tau_{\max}$ . For the case of plastics/metal interfaces based on BKV 130 H2.0 and steel, these four parameters were determined in our previous work (Grujicic et al., submitted for publication-b).

The interface decohesion potential presented above is next incorporated into a *User Element Library* (UEL) subroutine of Abaqus/Standard. The UEL subroutine allows the user to define the contribution of the interfacial elements to the global finite element model. In other words, for the given nodal displacements of the interface elements provided to UEL by ABAQUS, the contribution of the elements to the global vector

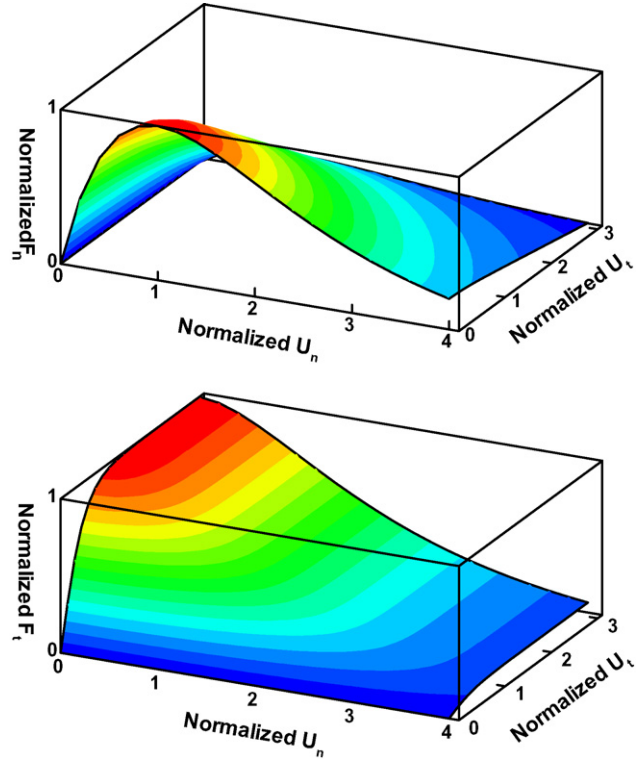


**Fig. A1 – Normalized normal,  $F_n$ , and tangential components,  $F_t$ , of the traction per unit interface area, as a function of the normalized normal,  $U_n$ , and normalized tangential,  $U_t$ , components of the interface displacements.**

of residual forces and to the global Jacobian (element stiffness matrix) is computed in the UEL subroutine and passed back to Abaqus/Standard. The implementation of the interface decohesion potential in the UEL subroutine is discussed below.

For the two-dimensional case presented here, each interface element is defined as a four-node iso-parametric element on the plastics/metal interface, as shown schematically in Fig. A2. In the un-deformed configuration (not shown for brevity), nodes 1 and 4, and nodes 2 and 3 coincide, respectively. A local co-ordinate system, consistent with the directions that are tangent,  $t$ , and normal,  $n$ , to the interface, is next assigned to the each element. This is done by introducing two internal nodes, A and B, located at the mid-points of the lines 1–2 and 3–4, connecting the corresponding interface nodes of the plastics and the metal. The interface displacements at the internal nodes A and B are expressed in terms of the displacements of the element nodes 1–4 as in the global coordinate system  $z$ - $r$ , as

$$U_n^A = (U_z^4 - U_z^1) \cos \theta - (U_r^4 - U_r^1) \sin \theta \quad (\text{A8})$$

$$U_t^A = (U_z^4 - U_z^1) \sin \theta - (U_r^4 - U_r^1) \cos \theta \quad (\text{A9})$$

$$U_n^B = (U_z^3 - U_z^2) \cos \theta - (U_r^3 - U_r^2) \sin \theta \quad (\text{A10})$$

$$U_t^B = (U_z^3 - U_z^2) \sin \theta - (U_r^3 - U_r^2) \cos \theta \quad (\text{A11})$$

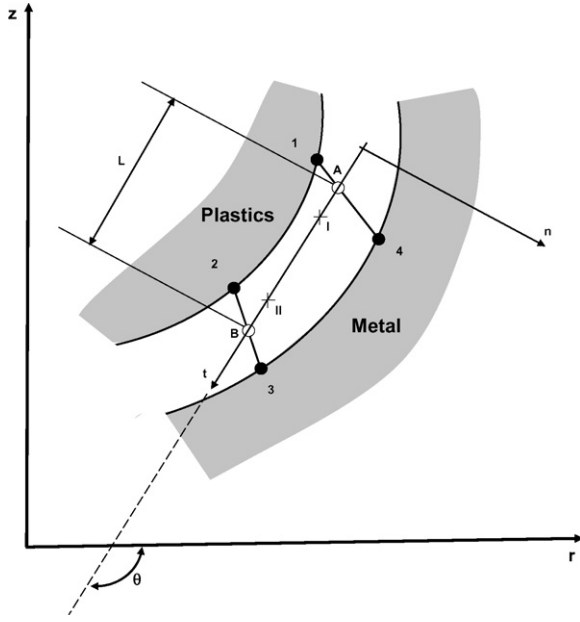


**Fig. A2 – Definition of the linear, four-node axisymmetric interface element. Nodes 1 and 4 and nodes 2 and 3 coincide in the equilibrium (reference) configuration. Internal nodes A and B located at the midpoints of segments connected corresponding nodes in the metal and plastics sides of the interface; two integration points marked as + and a local t–n co-ordinate system are also indicated.**

An iso-parametric coordinate  $\eta$  is next introduced along the tangent direction with  $\eta(A)=-1$  and  $\eta(B)=1$  and two linear Lagrangian interpolation functions are defined as  $N_A(\eta) = (1-\eta)/2$  and  $N_B(\eta) = (1+\eta)/2$ . These interpolation functions allow the normal and the tangential components of the interface displacements to be expressed in the form of their values at the internal nodes A and B as

$$U_t(\eta) = N_A(\eta)U_t^A + N_B(\eta)U_t^B \quad (A12)$$

$$U_n(\eta) = N_A(\eta)U_n^A + N_B(\eta)U_n^B \quad (A13)$$

The tangential and normal components of the forces at nodes A and B, i.e.  $F_t^A$ ,  $F_t^B$ ,  $F_n^A$  and  $F_n^B$ , which are work conjugates of the corresponding nodal displacements  $U_t^A$ ,  $U_t^B$ ,  $U_n^A$  and  $U_n^B$  are next determined through the application of the virtual work to the interfacial element as

$$\int_{-1}^1 \delta\Phi(\eta)L\pi r(\eta) d\eta = \sum_{I=n,t} \sum_{N=A,B} F_I^N \delta U_I^N \quad (A14)$$

where  $L$  is the A–B element length. The perturbation of interface potential is next expressed in terms of the perturbations of the interface displacements at the internal nodes A and B,  $U_t^A$ ,  $U_t^B$ ,  $U_n^A$ , and  $U_n^B$  as

$$\begin{aligned} \delta\Phi = & \frac{\partial\Phi[U_t(\eta), U_n(\eta)]}{\partial U_n} [N_A(\eta)\delta U_n^A + N_B(\eta)\delta U_n^B] \\ & + \frac{\partial\Phi[U_t(\eta), U_n(\eta)]}{\partial U_t} [N_A(\eta)\delta U_t^A + N_B(\eta)\delta U_t^B] \end{aligned} \quad (A15)$$

By substituting Eq. (A15) into Eq. (A14) and by choosing one of the  $\delta U_I^N$  ( $N = A, B; I = t, n$ ) perturbations at a time to be unity and the remaining perturbations to be zero, the corresponding  $F_I^N$  component of the nodal force can be expressed as

$$F_I^N = \int_{-1}^1 \frac{\partial\Phi[U_t(\eta), U_n(\eta)]}{\partial U_I} N_N(\eta)L\pi r(\eta) d\eta \quad (A16)$$

Using a straightforward geometrical procedure and imposing the equilibrium condition, the corresponding residual nodal forces  $R_r^i$  and  $R_z^i$  ( $i = 1-4$ ) in the global  $r$ - $z$  co-ordinate system, are defined as

$$\begin{aligned} R_r^1 = -R_r^4 = F_t^A \cos\theta - F_n^A \sin\theta, \quad R_z^1 = -R_z^4 = F_t^A \sin\theta - F_n^A \cos\theta, \\ R_r^2 = -R_r^3 = F_t^B \cos\theta - F_n^B \sin\theta, \quad R_z^2 = -R_z^3 = F_t^B \sin\theta - F_n^B \cos\theta \end{aligned} \quad (A17)$$

The components of the interface-element Jacobian are next defined as

$$\frac{\partial R_j^i}{\partial U_t^K} = \sum_{I=n,t} \sum_{N=A,B} \sum_{M=A,B} \frac{\partial R_j^i}{\partial F_t^N} \frac{\partial F_t^N}{\partial U_t^K} \frac{\partial U_t^M}{\partial U_t^K} \quad (A18)$$

where the components of the internal Jacobian  $\partial F_t^N / \partial U_t^M$  ( $i, j = n, t; N, M = A, B$ ) are calculated by differentiation of Eq. (A16).

To summarize, the residual nodal forces given by Eqs. (A17) and the element Jacobian given by Eq. (A18) are computed in the UEL subroutine, and passed to Abaqus/Standard for the use in its global Newton scheme for accurate assessment of the kinematics in the thermo-mechanical analysis of residual stress and interfacial decohesion development during polymer-to-metal direct-adhesion automotive-component manufacturing by injection molding.

## REFERENCES

- ABAQUS, 2006. Version 6.6. User Documentation. ABAQUS Inc., Rising Sun Mills, Providence, RI.
- Advani, S.G., Tucker III, C.L., 1987. The use of tensors to describe and predict fibers orientation in short fiber composites. *J. Rheol.* 31, 751–784.
- Altan, M.C., GuÈceri, S.I., Pipes, R.B., 1992. Anisotropic channel flow of fiber suspensions. *J. Non-Newtonian Fluid Mech.* 14, 65–83.
- Bird, R.B., Armstrong, R.C., Hassager, O., 1987. Dynamics of Polymeric Liquids: Fluid Mechanics, vol. 1., second ed. Wiley, New York.
- Bushko, W.C., Stokes, V.K., 1996. Solidification of thermoviscoelastic melts. Part 4. Effects of boundary conditions on shrinkage and residual stresses. *Polym. Eng. Sci.* 36, 658–675.
- Camacho, C.W., Tucker III, C.L., Yalvac, S., McGee, R.L., 1990. Stiffness and thermal expansion predictions for hybrid short fiber composites. *Polym. Compos.* 11, 229–239.
- CATIA, Version V5R16, Dassault Systems. [www.3ds.com](http://www.3ds.com).
- Crochet, M.J., Dupret, F., Verleye, V., 1994. In: Advani, S.G. (Ed.), *Flow and Rheology in Polymer Composites Manufacturing*, Ch. 11. Elsevier, Amsterdam.
- Doi, M., 1981. Molecular dynamics and rheological properties of concentrated solutions of rodlike polymers in isotropic and

- liquid crystalline phases. *J. Polym. Sci. Polym. Phys. Ed.* 19, 229–243.
- Eduljee, R.F., McCullough, R.L., Gillespie Jr., J.W., 1994. The influence of aggregated and dispersed textures on the elastic properties of discontinuous-fiber composites. *Comp. Sci. Technol.* 50, 381–391.
- Fan, X.J., Phan-Thien, N., Zheng, R., 1998. A direct simulation of fiber suspensions. *J. Non-Newtonian Fluid Mech.* 74, 113–136.
- Ferry, J.D., 1980. *Viscoelastic Properties of Polymers*, third ed. Wiley, New York.
- Folgar, F.P., Tucker, C.L., 1984. Orientation behaviour of fibers in concentrated suspensions. *J. Reinforced Plastics Compos.* 3, 98–119.
- Grujicic, M., Zhao, C.L., Dusel, E.C., 2005. The effect of thermal contact resistance on heat management in the electronic packaging. *Appl. Surf. Sci.* 246, 290–302.
- Grujicic, M., Sellappan, V., Arakere, G., Seyr, N., Erdmann, M. (in press). Computational feasibility analysis of direct-adhesion polymer-to-metal hybrid technology for load-bearing body-in-white structural components, *J. Mater. Process. Technol.*, doi:10.1016/j.jmatprotec.2007.05.016.
- Grujicic M., Sellappan V., Omar, M.A., Seyr, N., Erdmann, M. (submitted for publication-a). An overview of the polymer-to-metal direct-adhesion hybrid technologies for load-bearing automotive components. *Mater. Process. Technol.*
- Grujicic, M., Arakere, G., Mears, L., Seyr, N., Erdmann, M. (submitted for publication-b). Application of topology, size and shape optimization methods in polymer metal hybrid structural lightweight engineering, *Multidiscipline Model. Mater. Struct.*
- Guell, D., Lovalenti, M., 1995. An examination of assumptions underlying the state of the art in injection molding modeling. *SPE ANTEC* 95 (1), 728–732.
- Halpin, J.C., Kardos, J.L., 1976. The Halpin-Tsai equations: a review. *Polym. Eng. Sci.* 16, 344–352.
- Hypermesh, Altair Engineering Inc. [www.altair.com](http://www.altair.com).
- Jeffery, G.B., 1922. The motion of ellipsoidal particles immersed in viscous fluid. *Proc. Roy. Soc. Lond. A* 102, 161–179.
- Lipscomb II, G.G., Denn, M.M., Hur, D.U., Boger, D.V., 1988. The flow of fiber suspensions in complex geometry. *J. Non-Newtonian Fluid Mech.* 26, 297–325.
- MATLAB, 2006. *The Language of Technical Computing*, seventh ed. The MathWorks Inc., MA.
- Moldflow Plastics Insight, 2006. Version 6.1, User Documentation, Moldflow Corporation, Framingham, MA.
- Needleman, A., 1987. A continuum model for void nucleation by inclusion debonding. *J. Appl. Mech.* 54, 525–531.
- Papathanasiou, T.D., Guell, D.C. (Eds.), 1997. *Flow-induced Alignment in Composite Materials*. Woodhead, Cambridge, UK.
- Phan-Thien, N., Graham, A.L., 1991. A new constitutive model for fiber suspensions: flow past a sphere. *J. Rheol.* 30, 44–57.
- Phan-Thien, N., Zheng, R., 1997. Macroscopic modelling of the evolution of fibers orientation during flow. In: Papathanasiou, T.D., Guell, D.C. (Eds.), *Flow-Induced Alignment in Composite Materials*, Ch. 3. Woodhead, Cambridge, UK.
- Phan-Thien, N., Zheng, R., Graham, A.L., 1991. The flow of a model suspension fluid past a sphere. *J. Stat. Phys.* 62, 1173–1195.
- Plastic-Metal Hybrid Material. <http://www.hbmedia.net/polymotive/polymotive/2003/01/articles/frontend1.shtml>.
- Recktenwald, D., 2005. Advanced adhesives foster hybrid structures. *Mach. Design* 77 (21), 124–126.
- Rezayat, M., Burton, T.E., 1990. A boundary-integral formulation for complex three-dimensional geometries. *Int. J. Numer. Meth. Eng.* 29, 263–273.
- Rosenberg, J., Denn, M.M., Keunings, R., 1990. Simulation of non-recirculating flows of dilute fiber suspensions. *J. Non-Newtonian Fluid Mech.* 37, 317–345.
- Schapery, R.A., 1968. Thermal expansion coefficients of composite materials based on energy principles. *J. Compos. Mater.* 2, 380–404.
- Socrate, S., 1995. *Mechanics of microvoid nucleation and growth in high-strength metastable austenitic steels*. PhD Thesis. Massachusetts Institute of Technology.
- Tanner, R.I., 1988. *Engineering Rheology*, second ed. Oxford Press, London.
- Tucker III, C.L., 1991. Flow regimes for fiber suspensions in narrow gaps. *J. Non-Newtonian Fluid Mech.* 39, 239–268.
- Yamane, Y., Kaneda, Y., Doi, M., 1994. Numerical simulation of semi-dilute suspensions of rodlike particles in shear flow. *J. Non-Newtonian Fluid Mech.* 54, 405–421.
- Zheng, R., 1991. *Boundary element methods for some problems in fluid mechanics and rheology*. PhD Thesis. University of Sydney, 1991.
- Zheng, R., Kennedy, P., Phan-Thien, N., Fan, X.J., 1999. Thermoviscoelastic simulation of thermally and pressure-induced stresses in injection molding for the prediction of shrinkage and warpage for fiber-reinforced thermoplastics. *J. Non-Newtonian Fluid Mech.* 84, 159–190.
- Zoellner, O.J., Evans, J.A., 2002. Plastic-metal hybrid. A new development in the injection molding technology. In: ANTEC 2002 Annual Technical Conference, San Francisco, CA, pp. 1–4.